Chaos

Synchronization in a multilevel network using the Hamilton–Jacobi–Bellman (HJB) technique

Cite as: Chaos **32**, 093133 (2022); https://doi.org/10.1063/5.0088880
Submitted: 21 February 2022 • Accepted: 29 August 2022 • Published Online: 26 September 2022

Thierry Njougouo, Victor Camargo, Patrick Louodop, et al.

Synchronization in a multilevel network using the Hamilton–Jacobi–Bellman (HJB) technique

Cite as: Chaos **32**, 093133 (2022); doi: 10.1063/5.0088880
Submitted: 21 February 2022 · Accepted: 29 August 2022 ·
Published Online: 26 September 2022

Thierry Njougouo,[1,2,3,a)] Victor Camargo,[4,5] Patrick Louodop,[1,3] Fernando Fagundes Ferreira,[4,5] Pierre K. Talla,[6] and Hilda A. Cerdeira[7]

AFFILIATIONS

[1]Research Unit Condensed Matter, Electronics and Signal Processing, University of Dschang, P.O. Box 67, Dschang, Cameroon
[2]Faculty of Computer Science, University of Namur, Rue Gandgagnage 21, 5000 Namur, Belgium
[3]MoCLiS Research Group, Dschang, Cameroon
[4]Center for Interdisciplinary Research on Complex Systems, University of Sao Paulo, Av. Arlindo Bettio 1000, 03828-000 São Paulo, Brazil
[5]Department of Physics–FFCLRP, University of São Paulo, Ribeirao Preto, SP 14040-901, Brazil
[6]L2MSP, University of Dschang, P.O. Box 67, Dschang, Cameroon
[7]Instituto de Física Teórica, São Paulo State University (UNESP), Rua Dr. Bento Teobaldo Ferraz 271, Bloco II, Barra Funda, 01140-070 São Paulo, Brazil

[a)]**Author to whom correspondence should be addressed:** thierrynjougouo@ymail.com

ABSTRACT

This paper presents the optimal control and synchronization problem of a multilevel network of Rössler chaotic oscillators. Using the Hamilton–Jacobi–Bellman technique, the optimal control law with a three-state variable feedback is designed such that the trajectories of all the Rössler oscillators in the network are optimally synchronized at each level. Furthermore, we provide numerical simulations to demonstrate the effectiveness of the proposed approach for the cases of one and three networks. A perfect correlation between the MATLAB and PSpice results was obtained, thus allowing the experimental validation of our designed controller and shows the effectiveness of the theoretical results.

Synchronization of chaotic systems is a fundamental problem of nonlinear science, which has attracted continuous interest over several decades.[1–4] Most studies conducted in complex systems and, particularly, in the control of network dynamics use linear (usually diffusive) coupling models to investigate the network dynamics.[2,5–9] This method is limited because it takes a very long time to achieve a stable synchronization regime. To solve this problem, we propose in this work to build an optimal controller in the case of a network of chaotic oscillators that will not only reduce the transient phase to achieve the desired synchronization state but it also reduces considerably the simulation time. This investigation is implemented both in the numerical study on MATLAB software and on the electronic circuits made with the PSpice software, and the results are identical in the case of one layer as well as the case of three layers studied in this work.

I. INTRODUCTION

The history of the synchronization of dynamical systems goes back to Christiaan Huygens in 1665,[2] and in the past three decades, it has become a subject of intensive research due to their various domains of applications in fields, such as mathematics, physics, biology, economics, technology, and engineering.[1–3,10–12] This phenomenon exists in the case of two coupled systems as well as a network.[2,5,13] In recent decades, several works based on the study of synchronization in complex networks have focused on the problem of orienting the network toward a collective state shared by all the units, but for the most part considering the coupling coefficient as the control parameter used to achieve this dynamic.[6–8,13]

After an initial period of characterization of the complex networks in terms of local and global statistical properties, attention was turned to the dynamics of their interacting units. A widely studied example of such behavior is synchronization of coupled

oscillators arranged into complex networks.[13] Synchronization can be found applications in communication systems, system's security, and secrecy or cryptography.[14,15]

The investigations on the behavior of the network cooperative systems (or multi-agent systems) have received extensive attention, mainly due to its widespread applications, such as mobile robots, spacecraft, networked autonomous team, sensor networks, etc.[16–18] In all these applications, whatever the field, the main idea is control. Based on the literature of the control, a wide variety of approaches have been developed to control the behavior of the systems in a network. Several methods have been proposed to achieve chaos synchronization, such as impulsive control, adaptive control, time-delay feedback approach, active control, sliding mode, pinning control, compound synchronization, nonlinear control,[19–26] etc. Most of the above methods were used to synchronize two identical chaotic systems using adaptive methods.

To control a system is to be able to perform the appropriate modification on its inputs in order to place the outputs in a desired state. Most studies conducted in complex systems and, particularly, in the control of network dynamics use linear (usually diffusive) coupling models to study network dynamics.[2,5–9] This method is limited because it takes a very long time to achieve synchronization, thus rendering simulations practically useless. To solve this problem, we propose to build an optimal controller in the case of a network of chaotic oscillators that will not only reduce the transient phase to achieve the desired behavior, but it also reduces considerably the simulation time. It is important to mention that this work completes the work of Rafikov and Balthazar[27] who initially presented the synchronization of two Rössler chaotic systems based on the Hamilton–Jacobi–Bellman (HJB) techniques.

The structure of the article is as follows: In Sec. II, the control of the dynamics of one network (sometimes called a patch) of 50 Rössler chaotic oscillators based on the formulation of the problem is introduced a theorem illustrating how to design the controllers is proven also in this section. In Sec. III, the HJB technique presented in Sec. II is extended to three networks of 50 Rössler chaotic oscillators. Then, in Sec. IV, we illustrate the implementation of the technique using electronic circuits for a small number of oscillators.

II. SYNCHRONIZATION OF A NETWORK OF RÖSSLER CHAOTIC OSCILLATORS

The purpose of this section is to introduce a development optimal control law to resolve for the optimal synchronization of Rössler chaotic oscillators. The optimal control law is obtained using the Hamilton–Jacobi–Bellman (HJB) technique.[27,28]

A. Problem formulation

First, we present the model of a single network. Figure 1 shows the topology of connections between the nodes of the network.

Let us consider the well-known Rössler system[9,29] as the node dynamics with the following mathematical description of Eq. (1):

$$\begin{cases} \dot{x}_i^1 = -x_i^2 - x_i^3, \\ \dot{x}_i^2 = x_i^1 + a x_i^2, \\ \dot{x}_i^3 = b x_i^1 + x_i^3 (x_i^1 - c), \end{cases} \qquad i = 1, 2, \ldots, N, \tag{1}$$

where $a = 0.36$, $b = 0.4$, and $c = 4.5$.

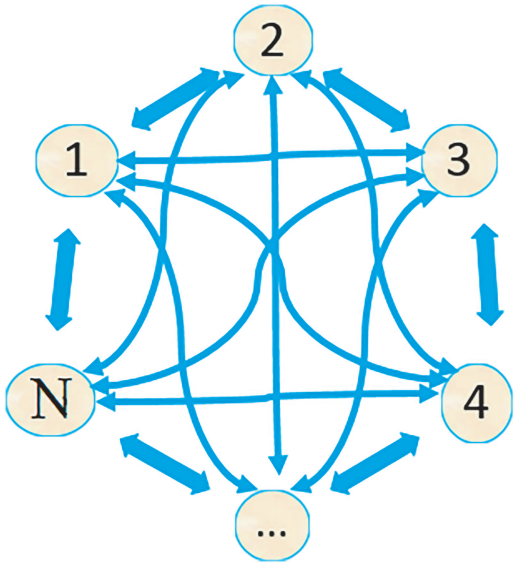

FIG. 1. Representation of the model of a single network.

The system has a zero bounded volume, globally attracting set.[30,31] Hence, for all time $t > 0$, the state trajectories $X_i(t) = (x_i^1(t), x_i^2(t), x_i^3(t))$ are globally bounded and continuously differentiable with respect to time t. Therefore, N positive constants L_i for all the N nodes of the network exist such that

$$||X_i|| \leq L_i \leq L_{max}, \quad i = 1, 2, \ldots, N, \tag{2}$$

where $||X_i||$ is the norm of the system identified by the index i, L_i is the maximum constant for the node i, and $L_{max} < \infty$ is the maximum constant for all nodes in the network.

Our goal is to develop an optimal control $u_i(t)$ to guarantee the complete synchronization of all systems in the network. We assume that the controlled model is defined by Eq. (3):

$$\dot{X}_i = f(X_i) + B u_i, \tag{3}$$

where $f(X_i)$: $\Re^n \to \Re^n$ represents the self-dynamics of node i [see Eq. (1)] of the network and $B \in \Re^{n \times m}$. Taking into account the controller $u_i \in \Re^m$, the dynamics of the network becomes

$$\begin{cases} \dot{x}_i^1 = -x_i^2 - x_i^3 + u_i^1, \\ \dot{x}_i^2 = x_i^1 + a x_i^2 + u_i^2, \\ \dot{x}_i^3 = b x_i^1 + x_i^3 (x_i^1 - c) + u_i^3. \end{cases} \qquad i = 1, 2, \ldots, N, \tag{4}$$

As mentioned previously, the goal is to design an appropriate optimal controller u_i^k ($k = 1, 2, 3$ and $i = 1, 2, \ldots, N$) such that for any initial condition, we have

$$\lim_{t \to \infty} \|e_{ij}\| = \lim_{t \to \infty} \|X_i(t) - X_j(t)\| = 0, \tag{5}$$

where $\|.\|$ represents the Euclidean norm and e_{ij} the error between system i and system j defined by $e_{ij}(t) = X_i(t) - X_j(t)$. Therefore, the dynamical system error between node i and node j is calculated

as follows:

$$\begin{cases} \dot{e}_{ij}^1 = -e_{ij}^2 - e_{ij}^3 + u_{ij}^1, \\ \dot{e}_{ij}^2 = e_{ij}^1 + a e_{ij}^2 + u_{ij}^2, \\ \dot{e}_{ij}^3 = b e_{ij}^1 + x_j^1 e_{ij}^3 + x_j^3 e_{ij}^1 + e_{ij}^1 e_{ij}^3 - c e_{ij}^3 + u_{ij}^3. \end{cases} \tag{6}$$

Clearly, the optimal synchronization problem is now replaced by the equivalent problem of optimally stabilizing the error system [Eq. (6)] using a suitable choice of the controllers u_{ij}^1, u_{ij}^2, and u_{ij}^3. In order to generalize Rafikov and Balthazar's work[27] to apply for a network, we prove that

Theorem 2.1. *The controlled Rössler chaotic oscillators presented by Eq. (4) will asymptotically synchronize provided the optimal controller u^* found minimizes the performance functional defined by Eq. (7),*

$$J = \int_0^\infty \Omega(e_{ij}^k, U)\, dt = \int_0^\infty \sum_{k=1}^{3} \sum_{i,j=1, i\neq j}^{N} \left(\alpha_{ij}^k \left(e_{ij}^k\right)^2 + \eta_{ij}^k \left(u_{ij}^k\right)^2 \right) dt. \tag{7}$$

Let $u_{ij}^k = -\frac{\lambda_{ij}^k}{\eta_{ij}^k} e_{ij}^k$ be the feedback controllers that minimize the above integral measure with λ_{ij}^k, η_{ij}^k, and α_{ij}^k being the weight of the links that satisfy the relationship $\alpha_{ij}^k = -\frac{\lambda_{ij}^k}{\eta_{ij}^k}$. The dynamical system error [Eq. (6)] converge to equilibrium $e_{ij}^k = 0$ ($k = 1, 2, 3$ and $i, j = 1, 2, \ldots, N$.).

Proof. Let us assume that the minimum of Eq. (7) is obtained with $U = U^* = \{u_1^{1*}, u_1^{2*}, u_1^{3*}; u_2^{1*}, u_2^{2*}, u_2^{3*}; \cdots; u_N^{1*}, u_N^{2*}, u_N^{3*}\}$. Therefore, we have

$$V(e_{ij}^k, U^*, t) = \min_U \int_0^\infty \Omega(e_{ij}^k, U_*, t)\, dt. \tag{8}$$

The function V may be treated as the Lyapunov function candidate.

Using the Hamilton–Jacobi–Bellman technique, we find the optimal controller U such that the system [Eq. (6)] is stabilized to equilibrium points and the integral [Eq. (7)] is minimum. Therefore, we have

$$\frac{\partial V}{\partial e_{ij}^1}\dot{e}_{ij}^1 + \frac{\partial V}{\partial e_{ij}^2}\dot{e}_{ij}^2 + \frac{\partial V}{\partial e_{ij}^3}\dot{e}_{ij}^3 + \sum_{k=1}^{3} \left(\alpha_{ij}^k \left(e_{ij}^k\right)^2 + \eta_{ij}^k (u_{ij}^{*k})^2 \right) = 0. \tag{9}$$

Replacing Eq. (6) into Eq. (9), we find

$$\begin{aligned} &\frac{\partial V}{\partial e_{ij}^1}\left(-e_{ij}^2 - e_{ij}^3 + u_{ij}^{*1}\right) + \frac{\partial V}{\partial e_{ij}^2}\left(e_{ij}^1 + a e_{ij}^2 + u_{ij}^{*2}\right) \\ &\quad + \frac{\partial V}{\partial e_{ij}^3}\left(b e_{ij}^1 + x_j^1 e_{ij}^3 + x_j^3 e_{ij}^1 + e_{ij}^1 e_{ij}^3 - c e_{ij}^3 + u_{ij}^{*3}\right) \\ &\quad + \sum_{k=1}^{3} \left(\alpha_{ij}^k \left(e_{ij}^k\right)^2 + \eta_{ij}^k (u_{ij}^{*k})^2 \right) = 0. \end{aligned} \tag{10}$$

The minimization of Eq. (10) with respect to U^* gives the following optimal controllers:

$$\frac{\partial V}{\partial e_{ij}^k} + 2\eta_{ij}^k u_{ij}^{*k} = 0 \Longrightarrow u_{ij}^{*k} = -\frac{1}{2\eta_{ij}^k}\frac{\partial V}{\partial e_{ij}^k}, \tag{11}$$

with $k = 1, 2, 3$ and $i, j = 1, 2, \ldots, N$.

Replacing Eq. (11) into Eq. (10), we obtain the following equation:

$$\begin{aligned} &\frac{\partial V}{\partial e_{ij}^1}\left(-e_{ij}^2 - e_{ij}^3\right) + \frac{\partial V}{\partial e_{ij}^2}\left(e_{ij}^1 + a e_{ij}^2\right) \\ &\quad + \frac{\partial V}{\partial e_{ij}^3}\left(b e_{ij}^1 + x_j^1 e_{ij}^3 + x_j^3 e_{ij}^1 + e_{ij}^1 e_{ij}^3 - c e_{ij}^3\right) \\ &\quad + \sum_{k=1}^{3} \left(\alpha_{ij}^k \left(e_{ij}^k\right)^2 - \frac{1}{2\eta_{ij}^k}\frac{\partial V}{\partial e_{ij}^k} \right) = 0. \end{aligned} \tag{12}$$

Now, considering

$$V(e_{ij}^k) = \sum_{k=1}^{3} \lambda_{ij}^k \left(e_{ij}^k\right)^2. \tag{13}$$

The Hamilton–Jacobi–Bellman relation described by Eq. (12) is satisfied. Therefore, the optimal controllers can be derived as follows:

$$u_{ij}^{*k} = -\frac{\lambda_{ij}^k}{\eta_{ij}^k} e_{ij}^k, \quad k = 1, 2, 3; \quad i, j = 1, 2, \ldots, N, \tag{14}$$

where the constants λ and η are positive. Differentiating the function in Eq. (13) along the optimal trajectories, we have

$$\dot{V}(e_{ij}^k) = -2\sum_{k=1}^{3} \alpha_{ij}^k \left(e_{ij}^k\right)^2 \leq 0. \tag{15}$$

Therefore, we can select V as a Lyapunov function. According to Refs. 22 and 32, this shows that the solutions of the system [Eq. (6)] are asymptotically stable in the Lyapunov sense via optimal control. □

B. Numerical simulation of the optimal synchronization in a single network

In order to demonstrate the effectiveness and validity of the proposed results in an optimal controller in the case of the network (patch) described in Eq. (4), we present and discuss the numerical results. We use MATLAB software with a fourth order Runge–Kutta integration method for numerical resolution of the non-linear differential equations.

We consider a network constituted by $N = 50$ Rössler chaotic oscillators with the optimal controllers obtained in Theorem 2.1. According to Ref. 33, the synchronization error of the whole network can be calculated using the relation given by

$$e(\mathbf{t}) = \frac{1}{N}\sum_{i,j=1}^{N} \left\| \mathbf{x}_i^k(\mathbf{t}) - \mathbf{x}_j^k(\mathbf{t}) \right\|. \tag{16}$$

In Fig. 2, we present the dynamics of the systems in the network without control. In Fig. 2(a), we can observe the dynamics of each

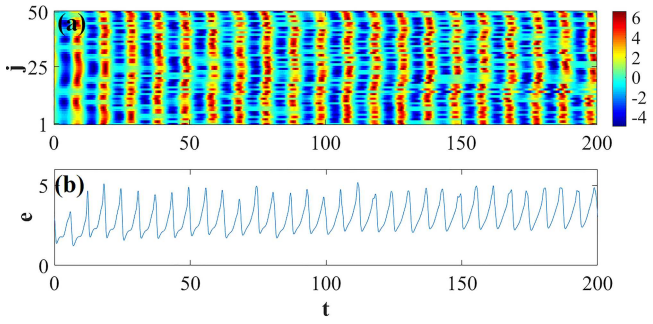

FIG. 2. Dynamics of the network without control: (a) Time series of the 50 oscillators showing the desynchronization of the oscillators of the patch. (b) Synchronization error between the oscillators of the patch. This result clearly shows that in the absence of the control, the systems of the network are in a state of total decoherence as shown by the error in (b).

oscillator of the network, and we conclude that synchronization does not exist here. This situation is confirmed in Fig. 2(b) by a non-zero synchronization error in this network. According to the literature, synchronization between chaotic oscillators is due to the presence of the coupling or control between these systems. Therefore, the results presented in Fig. 2 are normal because in the absence of any type of interaction or control, the existence of synchronization is a random fact.

Now, we proceed to demonstrate the effectiveness of the optimal control obtained in Theorem 2.1. In Fig. 3(a), we show the time series of synchronized elements for a network of Rössler chaotic oscillators for the constant parameters in the optimal controller: $\lambda_i = 1$ and $\eta_i = 10$ with $i = 1, 2, \ldots, N$. This chaotic synchronization is confirmed by the synchronization error plotted in Fig. 3(b). Therefore, it comes that the sum system is asymptotically stable.

Based on these results, it appears that this controller designed in Eq. (14) leads the systems of the network in a synchronous state with finite time. Therefore, it is important to evaluate the impact of these constant parameters appearing in optimal controllers on the time of synchronization of the systems of the network. Therefore, we present in Fig. 3(c) the synchronization errors of the network for three pairs of constant parameter values in the optimal controller where $\lambda_i = 1$ and $\eta_i = 100$ correspond to e_1 in red, $\lambda_i = 1$ and $\eta_i = 10$ correspond to e_2 in cyan, and $\lambda_i = 2$ and $\eta_i = 10$ correspond to e_3 in black. This figure leads us to conclude that when the constant parameter increases, the time required to reach synchronization decreases.

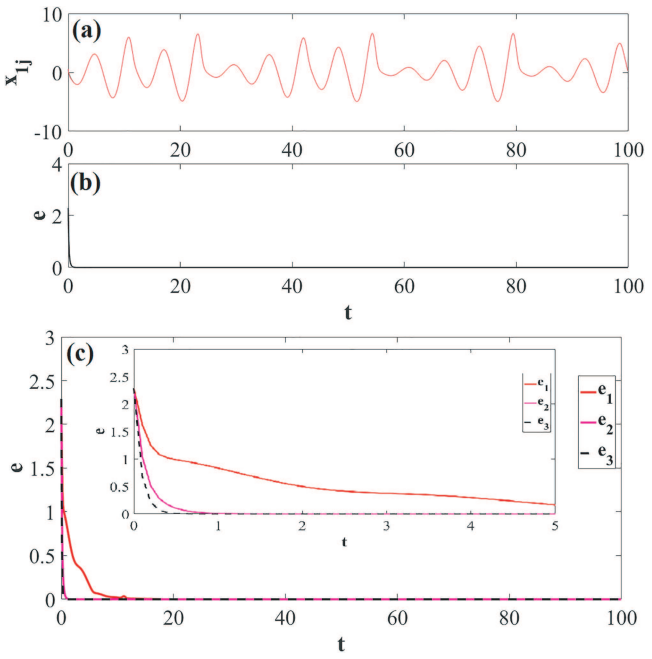

FIG. 3. Dynamics of the network with control: (a) Time series of the 50 oscillators showing the synchronization of the oscillators of the network. (b) Synchronization error between the oscillators of the network. (c) Error synchronization error between the oscillators of the network for some value of the control parameters.

III. DYNAMICS OF A MULTINETWORK WITH INTRANETWORK OPTIMAL CONTROL AND DIFFUSIVE COUPLING BETWEEN NETWORKS

In this section, we consider a model formed by three networks (see Fig. 4). Each network is made up of homogeneous (identical) systems but subject to different initial conditions. The main objective here is to show that the controller obtained previously remains optimal for intra-layer synchronization and that the control of the

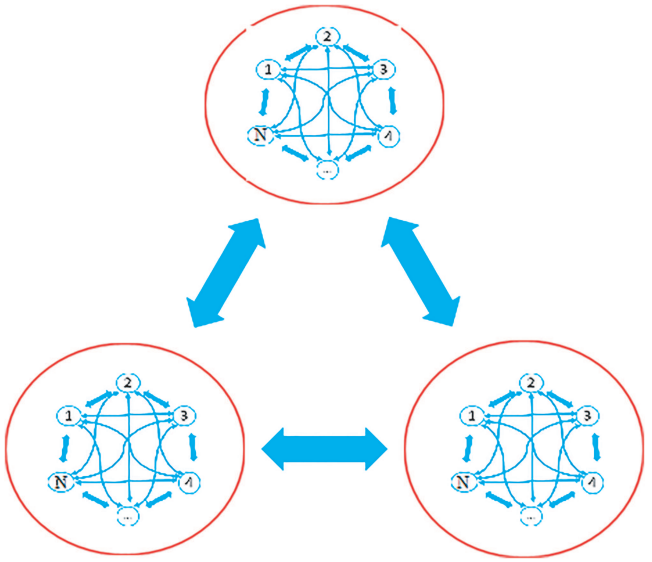

FIG. 4. Representation of the multi-network model.

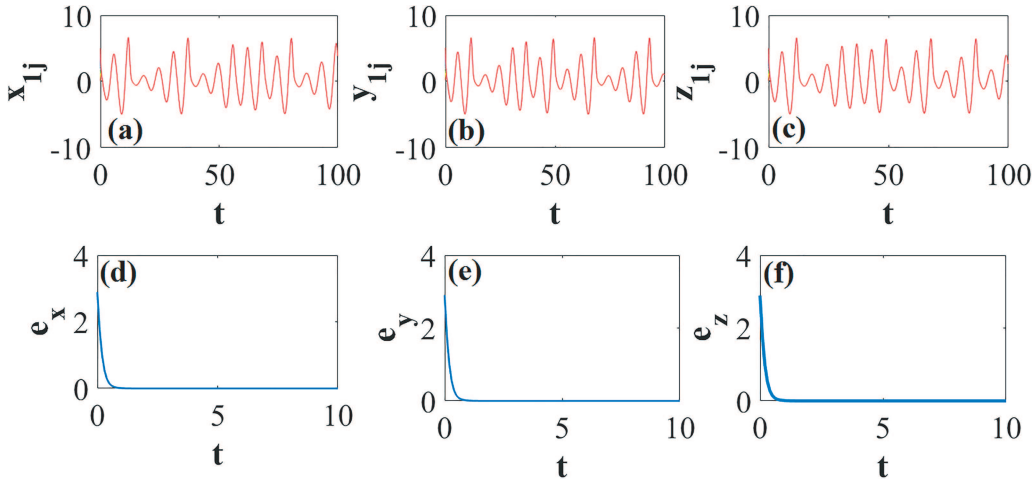

FIG. 5. Dynamics of each network with intra-network control: (a)–(c) Time series showing the synchronization of the oscillators of the first, second, and third network, respectively, for $\varepsilon_1 = \varepsilon_2 = \varepsilon_3 = 0$, $\lambda_i = 1$, and $\eta_i = 10$. (d)–(f) Synchronization errors between the oscillators of the first, second, and third network, respectively, for $\varepsilon_1 = \varepsilon_2 = \varepsilon_3 = 0$, $\lambda_i = 1$, and $\eta_i = 10$.

model toward a desired behavior comes down to the inter-layer coupling chosen diffusive.

In this representation, the mathematical description of each network is given as follows:

First network:

$$\begin{cases} \dot{x}_i^1 = -x_i^2 - x_i^3 + \chi_i^1 + \varepsilon_1 \left(y_i^1 + z_i^1 - 2x_i^1\right), \\ \dot{x}_i^2 = x_i^1 + a x_i^2 + \chi_i^2, \\ \dot{x}_i^3 = b x_i^1 + x_i^3 (x_i^1 - c) + \chi_i^3. \end{cases} \tag{17}$$

Second network:

$$\begin{cases} \dot{y}_i^1 = -y_i^2 - y_i^3 + v_i^1 + \varepsilon_2 \left(x_i^1 + z_i^1 - 2y_i^1\right), \\ \dot{y}_i^2 = y_i^1 + a y_i^2 + v_i^2, \\ \dot{y}_i^3 = b y_i^1 + y_i^3 (y_i^1 - c) + v_i^3. \end{cases} \tag{18}$$

Third network:

$$\begin{cases} \dot{z}_i^1 = -z_i^2 - z_i^3 + w_i^1 + \varepsilon_3 \left(x_i^1 + y_i^1 - 2z_i^1\right), \\ \dot{z}_i^2 = z_i^1 + a z_i^2 + w_i^2, \\ \dot{z}_i^3 = b z_i^1 + z_i^3 (z_i^1 - c) + w_i^3, \end{cases} \tag{19}$$

where $a = 0.36$, $b = 0.4$, and $c = 4.5$ are the system parameter and $i = 1, 2, \ldots, N$, where N is the number of elements in a single network. The state vector $X_i(x_i^1, x_i^2, x_i^3)$, $Y_i(y_i^1, y_i^2, y_i^3)$, and $Z_i(z_i^1, z_i^2, z_i^3)$ represent the first, second, and third patch, respectively. χ, v, and w are the intra-network optimal controllers of the first, second, and third network, respectively.

It is important to mention that these controllers are obtained without any inter-network connection. Therefore, based on Sec. II, the objective in all networks is the same, and the objective function

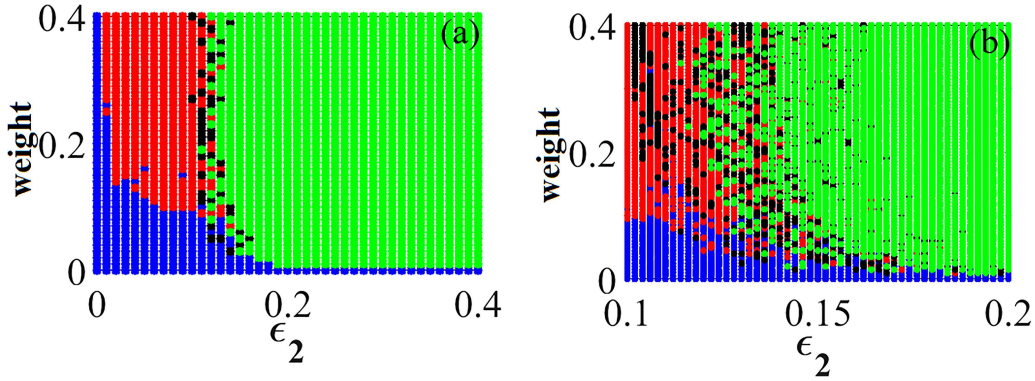

FIG. 6. (a) Dynamics of the three networks for $\lambda_{ij}^{*2} = 0.95$, $\eta_{ij}^{*2} = 10$, $\epsilon_1 = \epsilon_3 = 0.6$ and varying the weight in the first and third network as well as ϵ_2: the green zone represents where we have synchronization of all the networks in the network; the red domain delimits where we have the synchronization between the first and third network only; the black domain defines where we have synchronization in the first and third network, but in the second network, we have a disorder like a chimera state considering the whole network; the blue domain is where the synchronization of all networks in the network is not possible. (b) Zoom of Fig. 6(a) for ϵ_2 between 0.1 and 0.2.

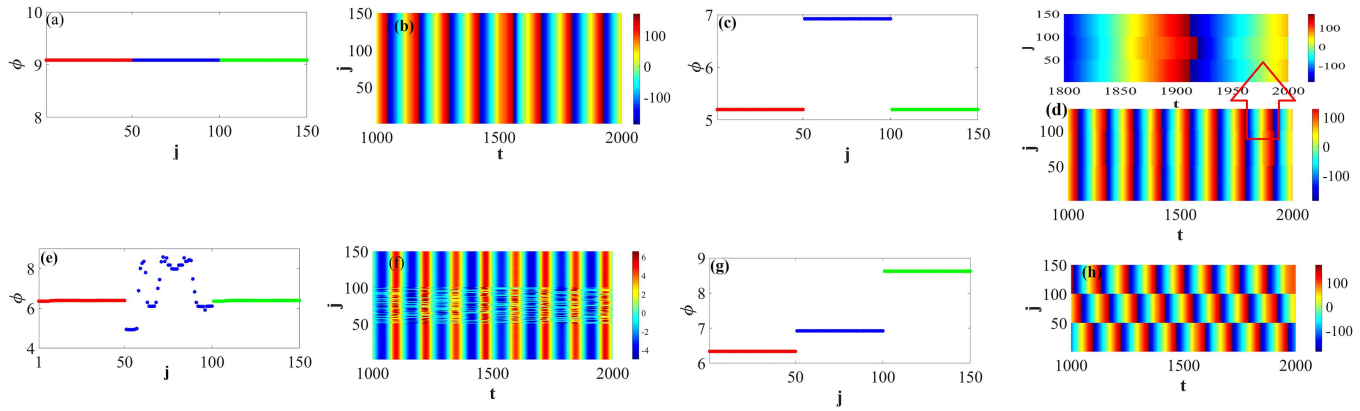

FIG. 7. Dynamics of the phases (expressed in degrees) and temporal dynamic of the whole network for $\lambda_{ij}^{*2} = 0.95$, $\eta_{ij}^{*2} = 10$, and $\epsilon_1 = \epsilon_3 = 0.6$. (a) and (b) One cluster formation for $\varepsilon_2 = 0.4$, $\lambda_{ij}^{*1,3} = 3$, and $\eta_i^{*1,3} = 10$. (c) and (d) Synchronization between Patches 1 and 3 (two cluster formations) for $\varepsilon_2 = 0.125$, $\lambda_{ij}^{*1,3} = 1.9$, and $\eta_i^{*1,3} = 10$. (e) and (f) Chimera like for $\varepsilon_2 = 0.11$, $\lambda_{ij}^{*1,3} = 1.9$, and $\eta_i^{*1,3} = 10$. (g) and (h) Three cluster formations for $\varepsilon_2 = 0.005$, $\lambda_{ij}^{*1,3} = 1$, and $\eta_i^{*1,3} = 10$.

for all these three networks is also the same. Following Theorem 2.1, the optimal controllers in each network will be defined as follows:

First network:

$$\chi_{ij}^{*k} = -\frac{\lambda_{ij}^k}{\eta_{ij}^k} e_{ij}^k, \quad k = 1,2,3; \quad i,j = 1,2,\ldots,N, \tag{20}$$

with $e_{ij}^k = x_i^k - x_j^k$, $\quad k = 1,2,3; \quad i,j = 1,2,\ldots,N$.

Second network:

$$v_{ij}^{*k} = -\frac{\lambda_{ij}^k}{\eta_{ij}^k} e_{ij}^k, \quad k = 1,2,3; \quad i,j = 1,2,\ldots,N, \tag{21}$$

with $e_{ij}^k = y_i^k - y_j^k$, $\quad k = 1,2,3; \quad i,j = 1,2,\ldots,N$.

Third network:

$$w_{ij}^{*k} = -\frac{\lambda_{ij}^k}{\eta_{ij}^k} e_{ij}^k, \quad k = 1,2,3; \quad i,j = 1,2,\ldots,N, \tag{22}$$

with $e_{ij}^k = z_i^k - z_j^k$, $\quad k = 1,2,3; \quad i,j = 1,2,\ldots,N$.

Using the optimal controllers presented in Eqs. (20)–(22) and without inter-network coupling ($\varepsilon_1 = \varepsilon_2 = \varepsilon_3 = 0$), we show in Fig. 5 the dynamics of each of the previously defined network. Figures 5(a)–5(c) show the time series of the first, second, and third network, respectively, and Figs. 5(d)–5(f) present the synchronization error in a much smaller time interval for good appreciation. These figures give a good indication of the validity of the proposed control.

Turning on the interlayer coupling in a multi-network modifies some parameters in the corresponding error. The calculations, although simple, are cumbersome due to the indexes involved; therefore, we test the performance of the proposed optimal control scheme through experimental simulations. We have left to the Appendix to show that the stability of the synchronization of the whole network depends on the intra-layer synchronization. This demonstration shows that the synchronization of the whole network is conditioned by the intra-layer synchronization. The simulations show that under the proposed control method, synchronization is achieved between all systems of all networks. We investigate simultaneously the impact of the coupling weight of the control and the inter-network coupling, and we obtain three different dynamics for the whole multilevel network, which we show in Fig. 6. These results are obtained under the following considerations: the weight in the second network is 0.095 ($\lambda_{ij}^{*2} = 0.95$ and $\eta_{ij}^{*2} = 10$) and the inter-network coupling is $\epsilon_1 = \epsilon_3 = 0.6$ in the first and third network. Thus, varying simultaneously the weights in the first and third networks as well as the internetwork coupling in the second network, we obtain four domains: first domain (green), where complete synchronization is achieved for all elements of the multilevel system as can be noted in Figs. 7(a) and 7(b). In Fig. 7, we represent the phase of the oscillators, calculated using the Hilbert transform and expressed in degrees defined as in Refs. 34 and 35 as well as a

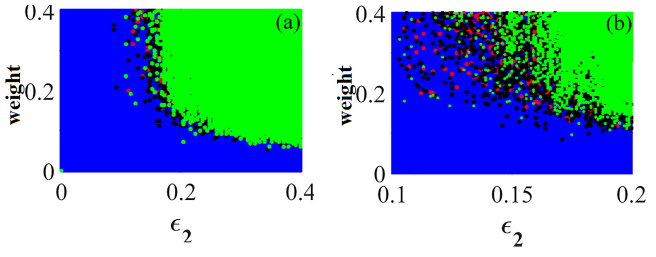

FIG. 8. (a) Dynamics of the three networks with N = 3 oscillators per network for $\lambda_{ij}^{*2} = 0.95$, $\eta_{ij}^{*2} = 10$, $\epsilon_1 = \epsilon_3 = 0.6$ and varying the weight in the first and third network as well as ϵ_2: the green zone represents where we have synchronization of all the networks in the network; the red domain delimits where we have the synchronization between the first and third network only; the black domain defines where we have synchronization in the first and third network, but in the second network, we have a disorder like a chimera state considering the whole network; the blue domain is where the synchronization of all networks in the network is not possible. (b) Zoom of Fig. 6(a) for ϵ_2 between 0.1 and 0.2.

three dimensional representation of the oscillator state to show the dynamics of the single oscillators in each of the phases shown in Fig. 6. In Figs. 7(a) and 7(b), the oscillators of these three networks form a single cluster. The second domain (red) indicates the region where the first and third networks synchronize. The particularity of this domain lies in the formation of two clusters as presented by Figs. 7(c) and 7(d), and all the three networks are internally completely synchronized. The black domain has practically the same properties as the previous red domain except that the second network shows a disordered state. This leaves the entire network to behave like a chimera as in Figs. 7(e) and 7(f). The last domain (blue) represents the parameter region when complete synchronization is not possible, while each single network is completely synchronized at different phase values, as shown in Figs. 7(g) and 7(h). The investigation of the stability of the synchronization in the whole network shows that this synchronization of the whole network is possible only if the systems synchronize first in the different layers as shown in the Appendix.

These studies show that the network can exhibit several behaviors depending on the parameters chosen.

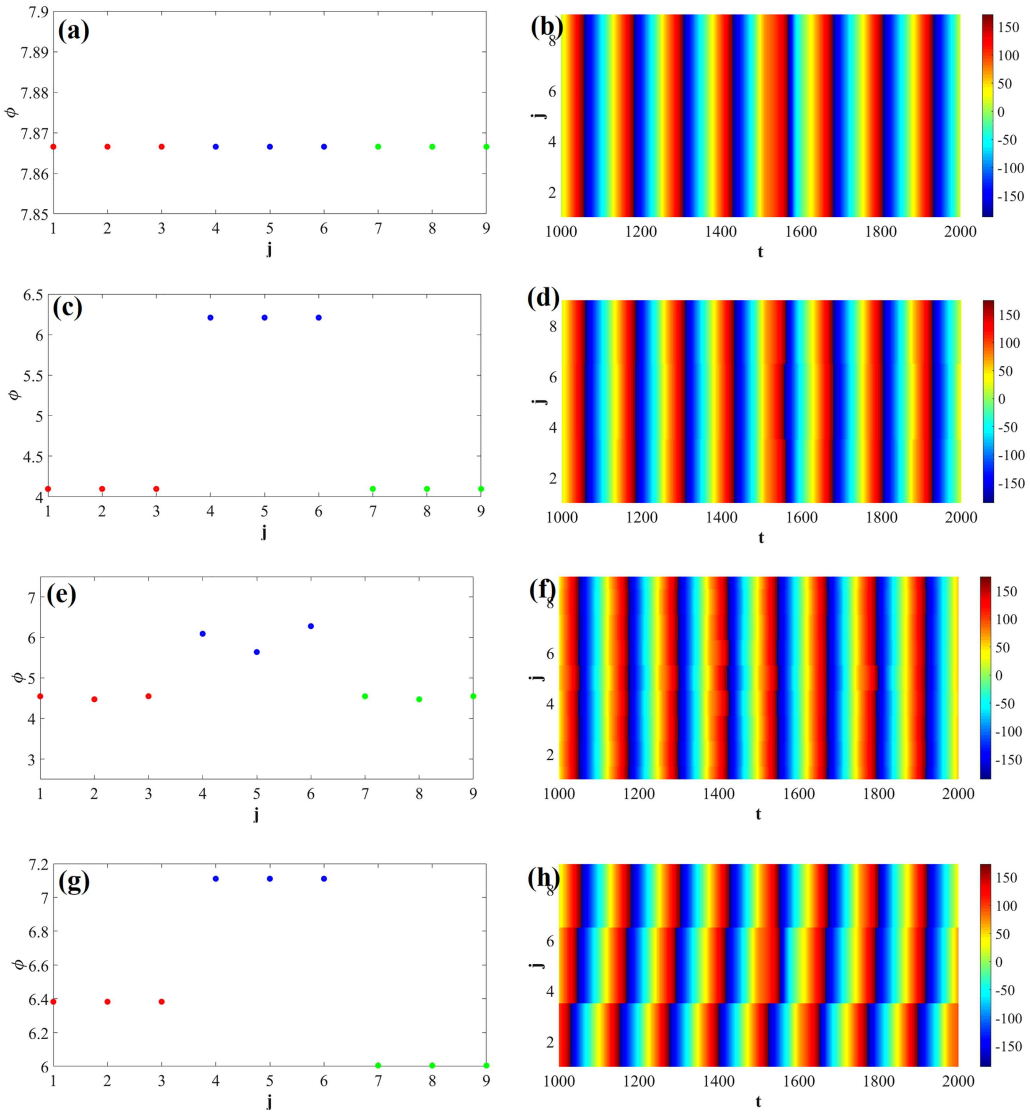

FIG. 9. Dynamics of the phases and temporal dynamic of the whole network for $\lambda_{ij}^{*2} = 0.95$, $\eta_{ij}^{*2} = 10$, and $\epsilon_1 = \epsilon_3 = 0.6$. (a) and (b) One cluster formation for $\varepsilon_2 = 0.4$, $\lambda_{ij}^{*1,3} = 3$, and $\eta_i^{*1,3} = 10$. (c) and (d) Synchronization between Patches 1 and 3 (two cluster formations) for $\varepsilon_2 = 0.115$, $\lambda_{ij}^{*1,3} = 2.6$, and $\eta_i^{*1,3} = 10$. (e) and (f) Chimera like for $\varepsilon_2 = 0.146$, $\lambda_{ij}^{*1,3} = 1.5$, and $\eta_i^{*1,3} = 10$. (g) and (h) Three cluster formations for $\varepsilon_2 = 0.005$, $\lambda_{ij}^{*1,3} = 1$, and $\eta_i^{*1,3} = 10$.

IV. CIRCUIT IMPLEMENTATION

In this section, we focus on implementing the networks as circuits, which can serve as a powerful tool to qualitatively describe quickly and cheaply the features that we want to demonstrate and, therefore, suggest devices for real experiments. For this implementation, we initially consider the case of one network with three Rössler oscillators and the study will extend to the case of three networks as in Sec. III. In order to better appreciate the experimental results that will be given later, we have redone the studies presented in Fig. 6 but now considering three oscillators per network (i.e., nine oscillators for the whole network). The results of this study are presented in Fig. 8, and like those of Fig. 6, they show the dynamics of the whole network for N = 3 oscillators per network.

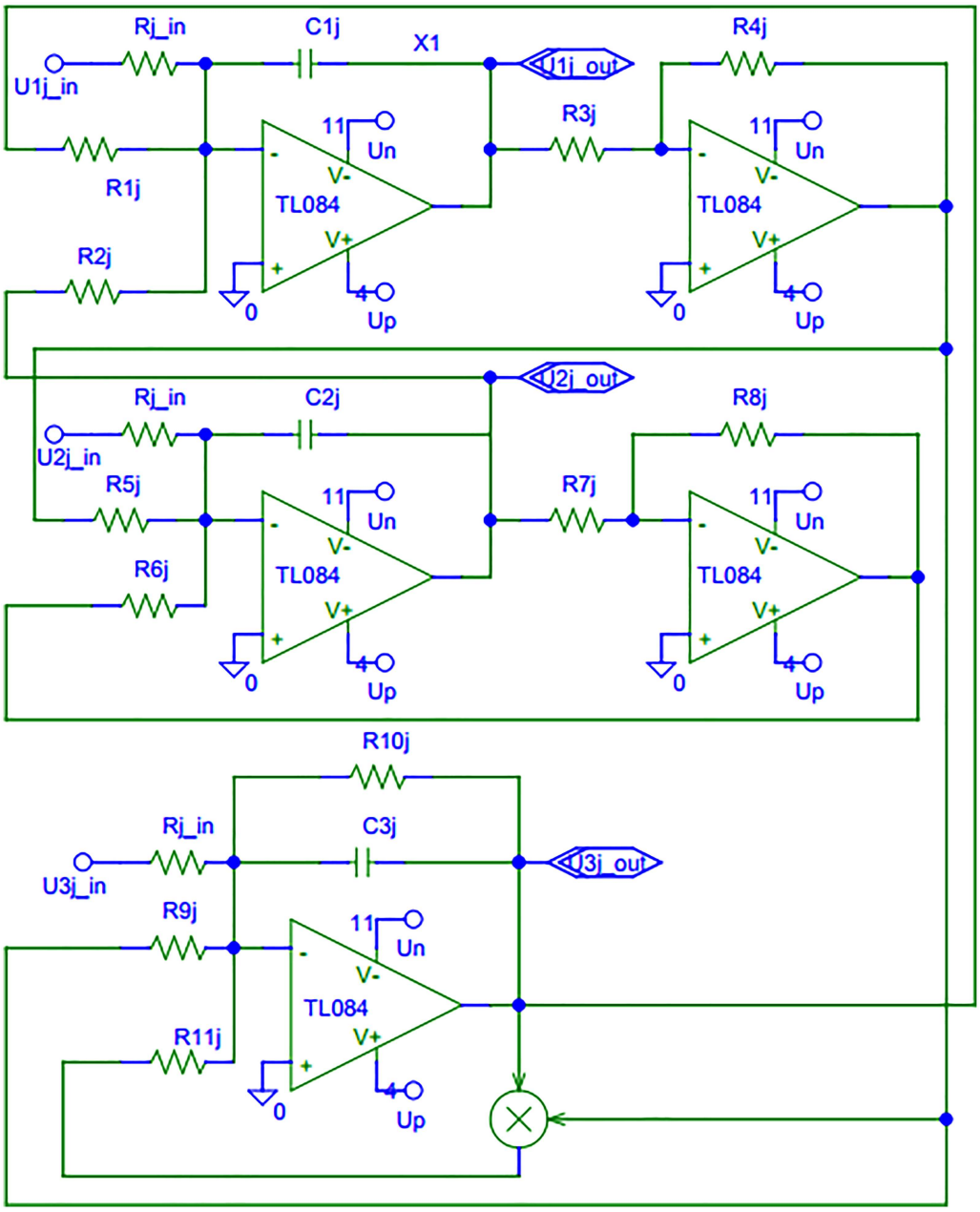

FIG. 10. Electronic circuit of the *j*th Rössler chaotic oscillators of the network.

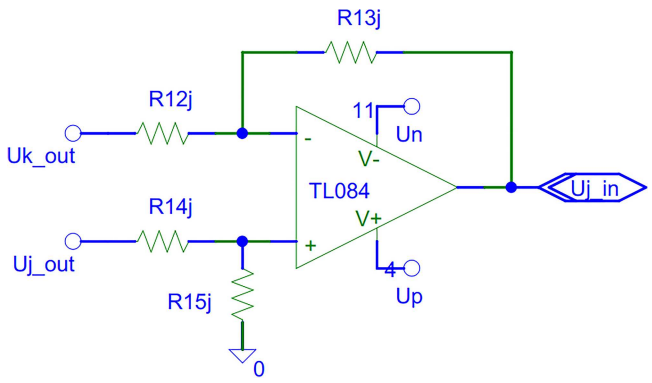

FIG. 11. Electronic circuit modeling the controller between the *j*th and *k*th oscillator analytically described by Eq. (14).

Figure 8 reproduces exactly the same dynamics as those observed in Fig. 6 for the same range of variation of the weight (which allows control of the intra-network dynamics) and the inter-network coupling (which controls the inter-network dynamics). The only difference is in the number of oscillators per patch.

Based on Fig. 8, we illustrate in Fig. 9 different behaviors, such as synchronization of these three networks [see Figs. 9(a) and 9(b)] presenting one cluster formation for the whole network. We can also have synchronization between the first and third network as it appears in Figs. 9(c) and 9(d), where the whole network presents two clusters. As illustrated in Figs. 7(e) and 7(f), the same result is reproduced for the case of three systems per network [see Figs. 9(e) and 9(f)]. In the same vein, we can mention the possibility of having three clusters in the network, and it only takes to make the inter-network coupling weak or null as recommended in Fig. 8 and where the snapshot is given in Figs. 9(g) and 9(h).

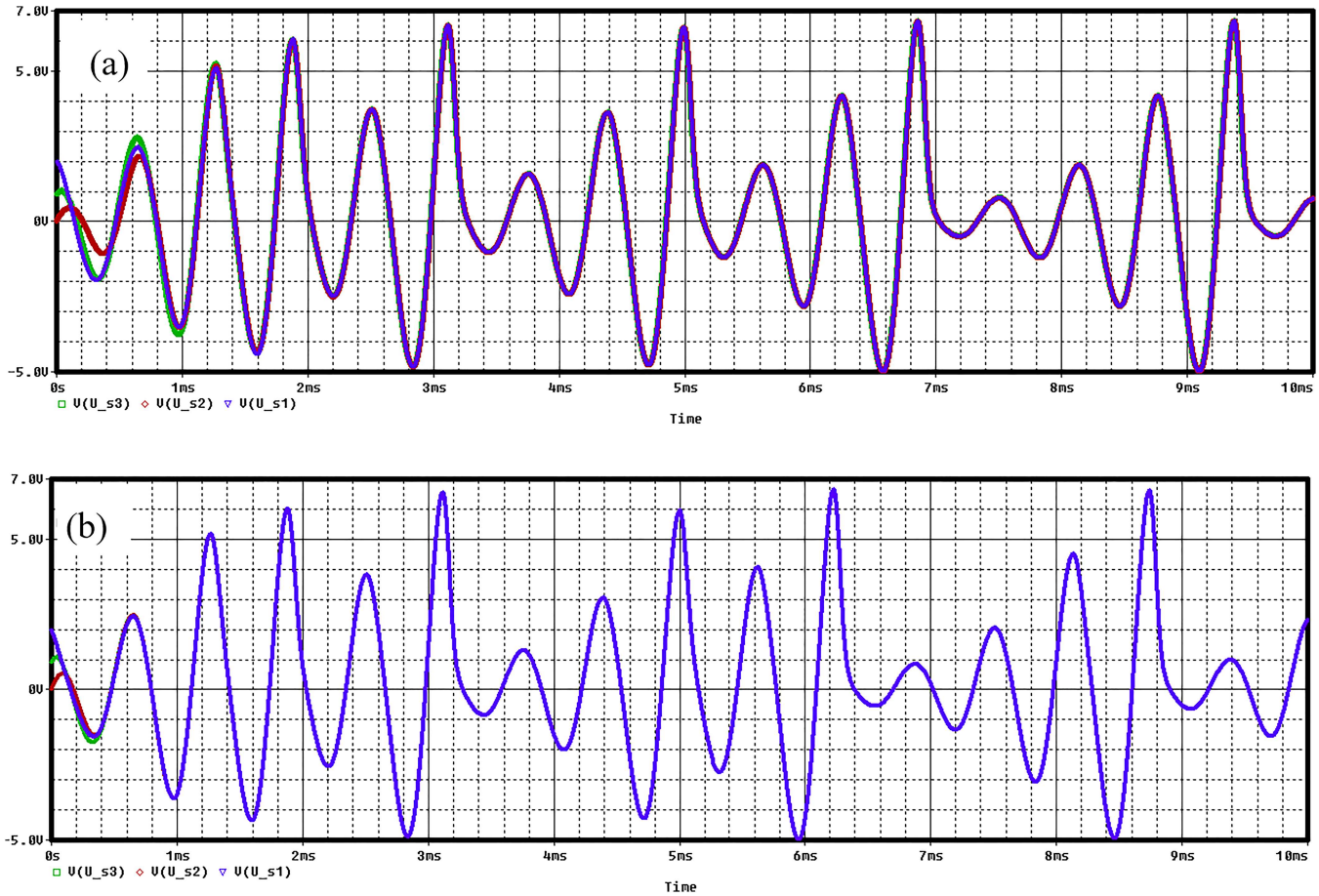

FIG. 12. PSpice results of the time series of the oscillators in one network with the controller of Fig. 11 for (a) $\lambda_i = 2$ and $\eta_i = 10$ and (b) $\lambda_i = 5$ and $\eta_i = 10$.

In Fig. 9, we represent the dynamics of the phases as well as the temporal dynamics of the whole network. The results presented in a way to be easily compared with Fig. 7 show that the experimental results follow closely those predicted by theory.

The goal of the next step is to design a suitable PSpice circuit simulator to investigate the systems described by Eqs. (4), (17), (18), and (19) with their controllers [Eqs. (14), (20), (21), and (22), respectively] in order to validate and support our theoretical results. However, the numerical solutions of the basic Rössler defined by Eq. (1) without a coupling term cannot be implemented using general circuit components due to the high amplitude of the signals that can destroy these components. In practice, it often needs to be varied to make proper adjustments to these variables.[36] Thus, the amplitude range of each variable value varies greatly. The working voltage range of electronic components is generally between $-15\,\mathrm{V}$ and $+15\,\mathrm{V}$ in practical electronic circuits. Therefore, implementing a synchronization strategy implies taking into consideration the constraints by saturation coming from the electronic components of the circuit.[37] The reason for this could be the high amplitudes (at least for a certain transient time) of the coupling functions that sometimes are really higher than the state variables of the systems.[37,38] Therefore, to implement the electronic circuit of our systems, we need to scale the variables of the systems. Thus, for the electrical equations, we choose $V^j_{x1}, V^j_{x2}, V^j_{x3}$ (with $j = 1, 2, \ldots, N$ being the index of the systems) as the state variables of the jth systems of the network of Rössler oscillators.

In order to avoid a very cumbersome presentation due to the amount of components of the circuit, we present in Fig. 10 only the circuit of one Rössler chaotic oscillator with $U_p = +15\,\mathrm{V}$ and $U_n = -15\,\mathrm{V}$ being the polarization voltages of the operational amplifiers used. In this circuit, $U_{1j}in$, $U_{2j}in$, and $U_{3j}in$ denote the inputs of the first, second, and third variable of the jth oscillator and $U_{1j}out$, $U_{2j}out$, and $U_{3j}out$ the outputs. Based on the previous transformation and using Kirchoff and Millmann laws, we present in Eq. (23) the circuit equations of the model presented previously in Eq. (4). The electronic circuit of the controller designed by Eq. (14) is given in Fig. 11 and their circuit equations by Eq. (24). For this implementation, the number of oscillators per network is $N = 3$,

$$\begin{cases} \dot{V}^j_{x_1} = \frac{1}{\xi C_{1j}}\left(-\frac{1}{R_{2j}}V^j_{x_2} - \frac{1}{R_{1j}}V^j_{x_3}\right) + \chi_i^{jk}, \\ \dot{V}^j_{x_2} = \frac{1}{\xi C_{2j}}\left(\frac{R_{4j}}{R_{3j}R_{5j}}V^j_{x_1} + \frac{R_{8j}}{R_{6j}R_{7j}}V^j_{x_2}\right) + \chi_i^{jk}, \\ \dot{V}^j_{x_3} = \frac{1}{\xi C_{3j}}\left(\frac{R_{4j}}{R_{3j}R_{9j}}V^j_{x_1} + V^j_{x_3}\left(\frac{R_{4j}}{R_{3j}R_{11j}}V^j_{x_1} - \frac{1}{R_{10j}}\right)\right) + \chi_i^{jk}, \end{cases} \tag{23}$$

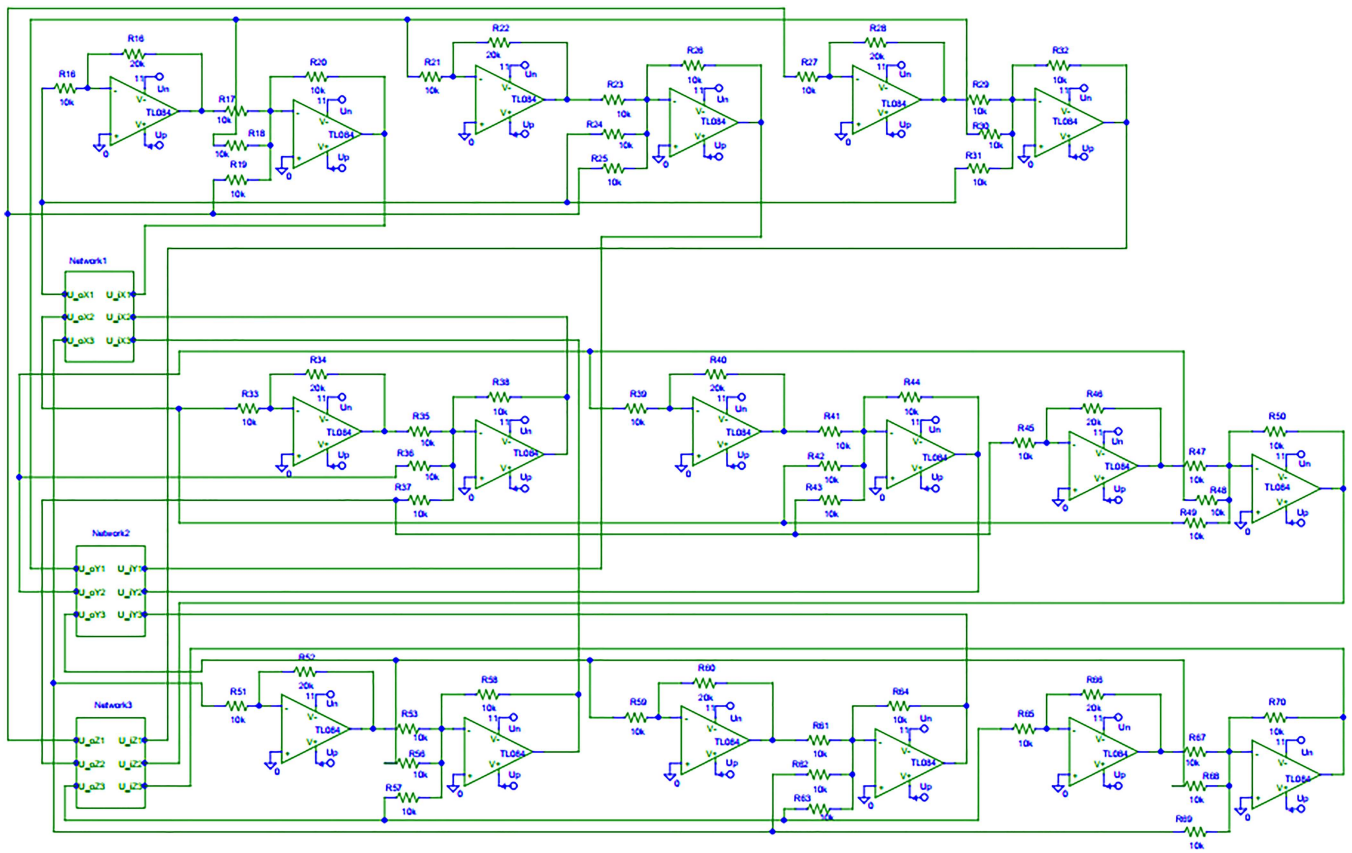

FIG. 13. Electronic circuit of three networks of Rössler chaotic oscillators with three oscillators per network.

with

$$\chi_i^{jk} = \frac{1}{\xi R_{in} C_{ij}} \left(\frac{R_{15j}}{R_{12j}} \left(\frac{R_{12j} + R_{13j}}{R_{14j} + R_{15j}} \right) U_{iout}^k - \frac{R_{13j}}{R_{12j}} U_{iin}^j \right), \quad (24)$$

where $V_x = \xi X$ and $\xi = 10^4$. After some mathematical calculations, we arrive at the following choice of component values: $C_{1j} = C_{2j} = C_{3j} = 10nF$, $R_{1j} = R_{2j} = R_{3j} = R_{4j} = 10\,\text{k}\Omega$, $R_{5j} = R_{7j} = R_{8j} = R_{11j} = 10\,\text{k}\Omega$, $R_{6j} = 27.8\,\text{k}\Omega$, $R_{9j} = 25\,\text{k}\Omega$, and $R_{10j} = 2.22\,\text{k}\Omega$. The values of the components used in Eq. (24) depend on the weight used previously: λ_{ij}^k, η_{ij}^k, and α_{ij}^k. The investigations of the effect of the weight on the transition to synchronization (presented in Fig. 3) are also checked using electronic circuits (see Fig. 10 for the electronic circuit of the jth oscillator in one network and Fig. 11 for the electronic circuit modeling the controller between the jth and kth oscillator). The simulation with the PSpice software of the whole circuit in the case of one network leads us to the results presented in Fig. 12 for two values of the weight. This result is captured directly from the graphical interface of the software PSpice for authenticity. In Fig. 12(a) where $\lambda_i = 2$ and $\eta_i = 10$, the computation of the values of the components of Fig. 11 leads to the following values: $R_{12j} = 50\,\text{k}\Omega$, $R_{13j} = 10\,\text{k}\Omega$, $R_{14j} = 50\,\text{k}\Omega$, $R_{15j} = 10\,\text{k}\Omega$, and $R_jin = 10\,\text{k}\Omega$. In Fig. 12(b), we have $R_{12j} = 20\,\text{k}\Omega$, $R_{13j} = 10\,\text{k}\Omega$, $R_{14j} = 20\,\text{k}\Omega$, $R_{15j} = 10\,\text{k}\Omega$, and $R_jin = 10\,\text{k}\Omega$ for $\lambda_i = 5$ and $\eta_i = 10$. This result shows not only the synchronization of the three circuits used in this network but also we can observe that when we increase the value of the weight, the transient time to obtain synchronization is reduced. Therefore, it confirms the effectiveness of the proposed control and the previous result [Fig. 3(c)] obtained in MATLAB.

For the case of three networks as presented in Fig. 4, we have decided to simplify the equations and have considered the general form given by

$$\dot{X}_i^j = f(X_i^j) + \chi_i^{jk} + \epsilon(X_i^{j-1} + X_i^{j+1} - 2X_i^j), \quad i = j = 1, 2, 3, \quad (25)$$

where χ and ϵ are, respectively, the optimal controllers obtained in each network and the coupling strength between the networks. Therefore, the electrical equations of each network can be expressed as follows:

$$\dot{V}_i^j = f(V_i^j) + \chi_i^{jk} + \epsilon(V_i^{j-1} + V_i^{j+1} - 2V_i^j), \quad i, j = 1, 2, 3. \quad (26)$$

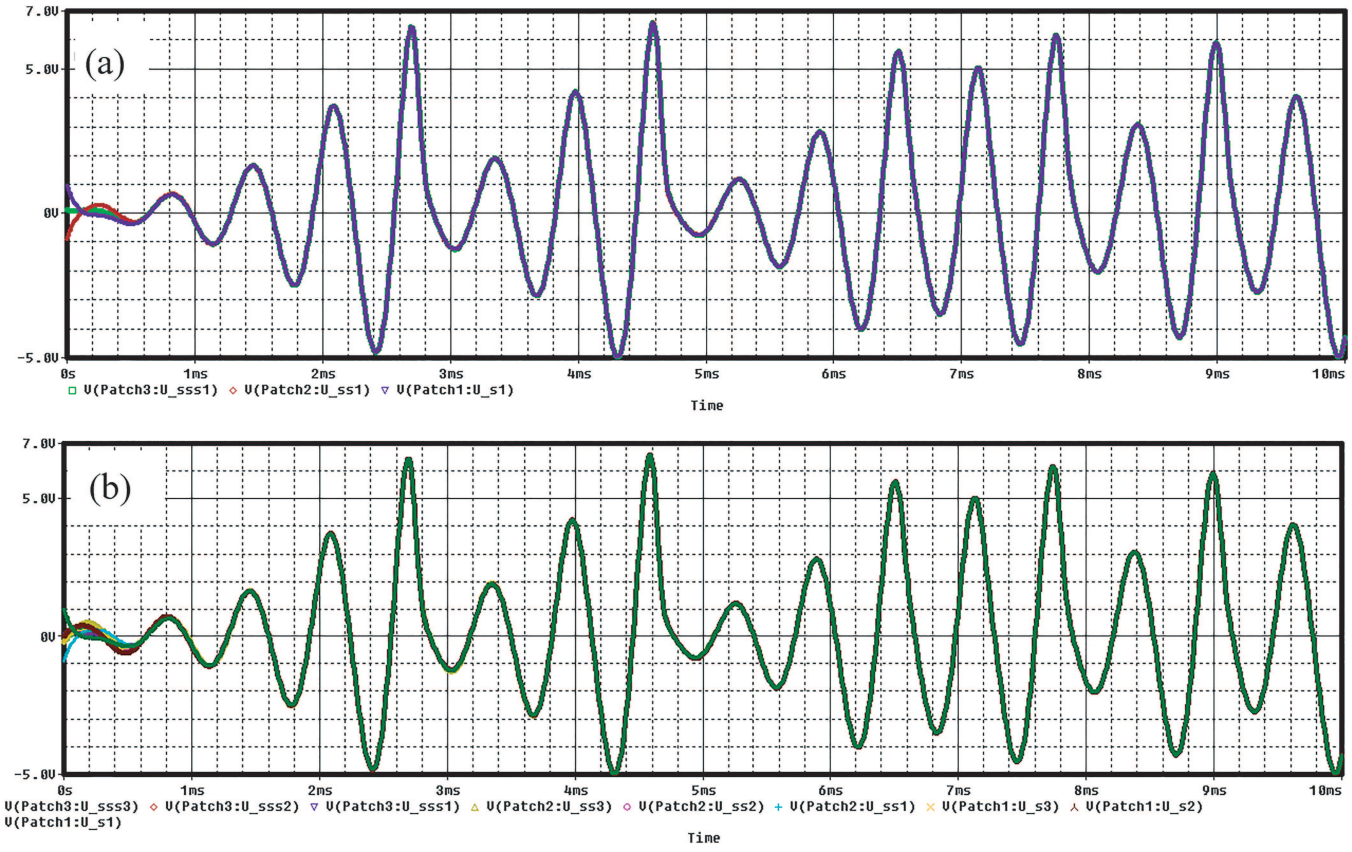

FIG. 14. PSpice results of the time series of the oscillators in the case of three networks: (a) time series of the first oscillators in each network and (b) time series of all the oscillators in each network for $\lambda_i = 5$, $\eta_i = 10$, and $\epsilon = 0.5$ ($i = 1, 2, 3$).

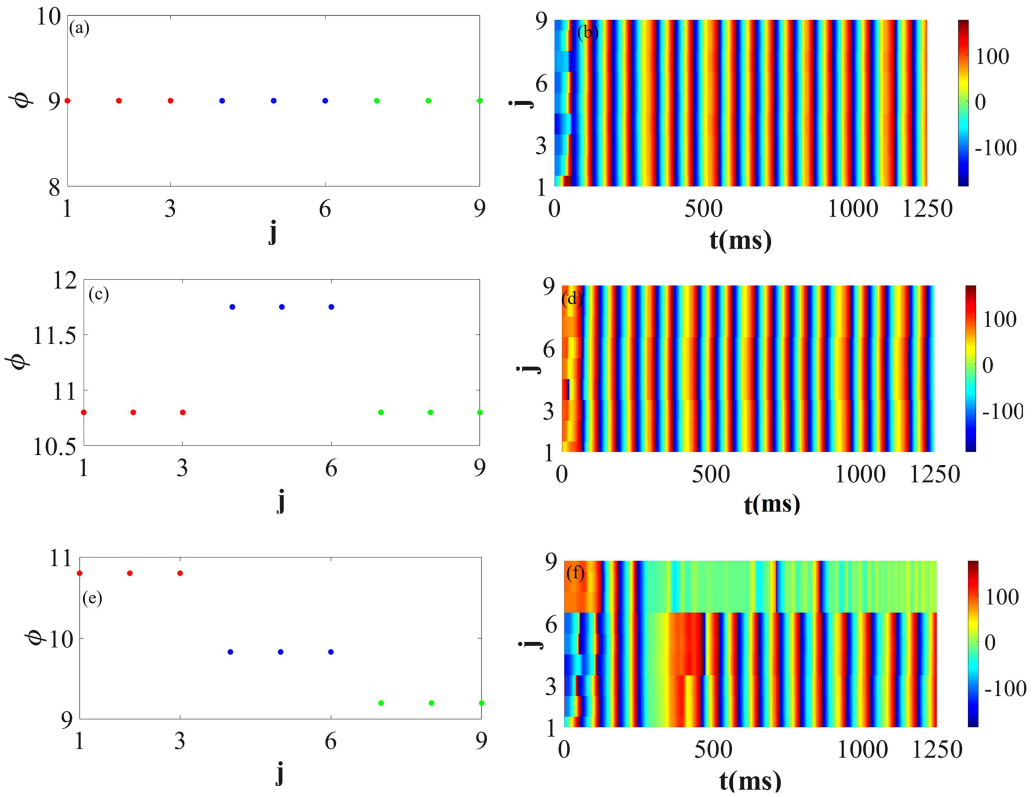

FIG. 15. PSpice results of the dynamics of the phases and temporal dynamics of the whole network corresponding to the parameter value of Fig. 9.

Equation (26) is obtained according to the elements (components) of Fig. 13 while respecting the values of the parameters given previously.

Figure 13 shows the circuit of the whole network of nine Rössler chaotic oscillators. This global network as mentioned above is formed by three oscillators per sub-network. Thus, in this figure, the boxes marked Network1, Network2, and Network3 represent, respectively, the first, second, and third network where the control laws and the systems are those given in Figs. 10 and 11. The diffusive couplings between the patches are represented in Fig. 13. The terminals U_iX_j, U_iY_j, and U_iZ_j represent the inputs of the three systems in each patch (network) and the terminals U_oX_j, U_oX_j and U_oX_j the corresponding outputs in each patch. The values of the resistances marked in this Fig. 13 correspond to $\epsilon = 0.5$ used previously in MATLAB simulation. After simulation in PSpice, we show in Fig. 14 the time series of the whole network constituted by 3N oscillators. In Fig. 14(a), we present the time series of the first oscillator of each network for $\lambda_i = 5$, $\eta_i = 10$, and $\epsilon = 0.5$. In Fig. 14(b), we show the time series of the nine oscillators of the whole network. Based on these results, we can confirm the effectiveness of our control in the case of three networks.

To further investigate and validate the experimental results, studies have been made using the circuit shown in Fig. 13. The results of these studies, which are presented in Fig. 15, allowed us to show the existence of the phenomena observed theoretically in MATLAB. Among these phenomena, we have the synchronization of the three networks [see Figs. 15(a) and 15(b)], the synchronization between Networks 1 and 3 [see Figs. 15(c) and 15(d)] and the formation of three clusters [Figs. 15(e) and 15(f)].

V. CONCLUSION

This paper presents a theoretical and experimental study (study performed under MATLAB and PSpice) in achieving optimal synchronization for a multi-level network of Rössler chaotic oscillators. An optimal controller was designed in this study first for the synchronization of a network (or a network) of 50 Rössler chaotic oscillators and second for the synchronization of three networks of 50 Rössler chaotic oscillators. The designed optimal control law satisfied Lyapunov's stability theorem and the HJB technique. It also shows under simulation that the control method we developed can guarantee a chaotic state for all the oscillators of the network at synchronization. Using this control method, it also demonstrates the possibility to obtain complete synchronization for the three networks, cluster formation, or a semblance of chimera state for the global network. Electronic circuits also show the effectiveness of the proposed method.

ACKNOWLEDGMENTS

T.N. thanks the University of Namur for the financial support. H.A.C. thanks ICTP-SAIFR and FAPESP (Grant No. 2016/01343-7) for partial support. P.L. acknowledges support by the FAPESP (Grant No. 2014/13272-1).

AUTHOR DECLARATIONS

Conflict of Interest

The authors have no conflicts to disclose.

DATA AVAILABILITY

The data that support the findings of this study are available within the article.

APPENDIX: STABILITY OF THE ALL NETWORK SYNCHRONIZATION

Let us consider the simultaneous synchronization error, from all the nodes in the multilevel network consisting of the coupled three layers, expressed as $\xi_i^k = x_i^k + y_i^k - 2z_i^k$, and the intra-layer couplings described by the following expressions:

$$\begin{cases} \chi_i^k = \sum_{j=1}^N \theta_{ij}\left(x_i^k - x_j^k\right), \\ \nu_i^k = \sum_{j=1}^N \theta_{ij}\left(y_i^k - y_j^k\right), \\ \omega_i^k = \sum_{j=1}^N \theta_{ij}\left(z_i^k - z_j^k\right), \end{cases} \tag{A1}$$

with $\theta_{ij}^k = \frac{\lambda_{ij}^k}{\eta_{ij}^k}$, $k = 1, 2, 3;\ i, j = 1, 2, \ldots, N$.

For simplicity, we chose $\varepsilon_k = \varepsilon$ for $k = 1, 2, 3$, and we consider that θ_{ij} are identical. Thus, the coupling between layers becomes $P = \varepsilon\left[y_i^1 + z_i^1 - 2x_i^1 + x_i^1 + z_i^1 - 2y_i^1 - 2\left(x_i^1 + y_i^1 - 2z_i^1\right)\right] = -3\varepsilon\xi_i^1$ and the intralayer coupling becomes:

$$I_i^k = \chi_i^k + \nu_i^k - 2\omega_i^k, \tag{A2}$$

$$I_i^k = -\sum_{j=1}^N \theta_{ij}^k\left(\xi_i^k - \xi_j^k\right). \tag{A3}$$

Considering the previous relations, we obtain the following error system:

$$\begin{cases} \dot{\xi}_i^1 = -\xi_i^2 - \xi_i^3 - \sum_{j=1}^N \theta_{ij}^1\left(\xi_i^1 - \xi_j^1\right) - 3\varepsilon\xi_i^1, \\ \dot{\xi}_i^2 = \xi_i^1 + a\xi_i^2 - \sum_{j=1}^N \theta_{ij}^2\left(\xi_i^2 - \xi_j^2\right), \\ \dot{\xi}_i^1 = b\xi_i^1 - c\xi_i^3 - \sum_{j=1}^N \theta_{ij}^3\left(\xi_i^3 - \xi_j^3\right) + G, \end{cases} \tag{A4}$$

where $G = x_i^3 x_i^1 + y_i^3 y_i^1 - 2z_i^3 z_i^1$.

The problem now is to prove the stability of the entire connected layers basing ourselves on the error system [Eq. (A4)]. To do so, let us select the following Lyapunov function as given by Eq. (A5):

$$v_i = \frac{1}{2}\left(\left(\xi_i^1\right)^2 + \left(\xi_i^2\right)^2 + \frac{1}{b}\left(\xi_i^3\right)^2\right). \tag{A5}$$

Its time derivative is expressed by the following equation (A6):

$$\dot{v}_i = -\sum_j^N \theta_{ij}\left(\left(\xi_i^1 - \xi_j^1\right)\xi_i^1 + \left(\xi_i^2 - \xi_j^2\right)\xi_i^2 + \frac{1}{b}\left(\xi_i^3 - \xi_j^3\right)\xi_i^3\right) - 3\varepsilon\left(\xi_i^1\right)^2 + a\left(\xi_i^2\right)^2 - \frac{c}{b}\left(\xi_i^3\right)^2 + \frac{G}{b}\xi_i^3. \tag{A6}$$

Considering that $\left|\frac{G}{b}\right| \le L\left|\xi_i^1\right|$, then $L\left|\xi_i^1\right|\left|\xi_i^3\right| \le \frac{L}{2}\left(\left(\xi_i^1\right)^2 + \left(\xi_i^3\right)^2\right)$.

Thus, relation [Eq. (A6)] becomes

$$\dot{v}_i \le -\sum_j^N \theta_{ij}\left(\left(\xi_i^1 - \xi_j^1\right)\xi_i^1 + \left(\xi_i^2 - \xi_j^2\right)\xi_i^2 + \frac{1}{b}\left(\xi_i^3 - \xi_j^3\right)\xi_i^3\right) - 3\varepsilon\left(\xi_i^1\right)^2 + a\left(\xi_i^2\right)^2 - \frac{c}{b}\left(\xi_i^3\right)^2 + \frac{L}{2}\left(\left(\xi_i^1\right)^2 + \left(\xi_i^3\right)^2\right) \tag{A7}$$

$$\dot{v}_i \le -\sum_j^N \theta_{ij}\left(\left(\xi_i^1 - \xi_j^1\right)\xi_i^1 + \left(\xi_i^2 - \xi_j^2\right)\xi_i^2 + \frac{1}{b}\left(\xi_i^3 - \xi_j^3\right)\xi_i^3\right) - \left(3\varepsilon - \frac{L}{2}\right)\left(\xi_i^1\right)^2 + a\left(\xi_i^2\right)^2 - \left(\frac{c}{b} - \frac{L}{2}\right)\left(\xi_i^3\right)^2 \tag{A8}$$

$$\dot{v}_i \le -\sum_j^N \theta_{ij}\left(\left(\xi_i^1 - \xi_j^1\right)\xi_i^1 + \left(\xi_i^2 - \xi_j^2\right)\xi_i^2 + \frac{1}{b}\left(\xi_i^3 - \xi_j^3\right)\xi_i^3\right) - \xi_i^T Q\xi_i, \tag{A9}$$

where

$$Q = \begin{pmatrix} \left(3\varepsilon - \frac{L}{2}\right) & 0 & 0 \\ 0 & -a & 0 \\ 0 & 0 & \left(\frac{c}{b} - \frac{L}{2}\right) \end{pmatrix}, \tag{A10}$$

$$\dot{v}_i \le -\sum_j^N \theta_{ij}\left(\left(\xi_i^1 - \xi_j^1\right)\xi_i^1 + \left(\xi_i^2 - \xi_j^2\right)\xi_i^2 + \frac{1}{b}\left(\xi_i^3 - \xi_j^3\right)\xi_i^3\right) - \lambda_{\min}(Q)\left\|\xi_i\right\|^2. \tag{A11}$$

From here, it comes out that the time derivative of the Lyapunov function in Eq. (A11) is negative if the nodes in each layer synchronize, namely, if for all i and j $\xi_i^k - \xi_j^k = 0$. Thus,

$$\dot{v}_i \le w(t), \tag{A12}$$

$$w(t) = -\lambda_{\min}(Q)\left\|\xi_i(t)\right\|^2. \tag{A13}$$

Integrating the preview equation from zero to t yields

$$w(0) \ge \int_0^t w(s)\, ds. \tag{A14}$$

As t goes to infinity, the above integral is always less than or equal to $w(0)$. Since $w(0)$ is positive and finite, $\lim_{t\to\infty}\int_0^t w(\tau)\,d\tau$ exists and is finite. Thus, according to the Barbalat lemma,[39] one obtains

$$\lim_{t\to\infty} w(t) = \lambda_{\min}(Q)\lim_{t\to\infty}\|\xi(t)\|^2 = 0, \tag{A15}$$

which implies that $\lim_{t\to\infty}\xi_i(t) = 0$. This achieves the proof.

REFERENCES

[1] E. Mosekilde, Y. Maistrenko, and D. Postnov, *Chaotic Synchronization: Applications to Living Systems* (World Scientific, 2002), Vol. 42.
[2] A. Pikovsky, J. Kurths, M. Rosenblum, and J. Kurths, *Synchronization: A Universal Concept in Nonlinear Sciences* (Cambridge University Press, 2003), Vol. 12.
[3] F. Dörfler, M. Chertkov, and F. Bullo, "Synchronization in complex oscillator networks and smart grids," Proc. Natl. Acad. Sci. U.S.A. **110**, 2005–2010 (2013).
[4] T. Weng, H. Yang, C. Gu, J. Zhang, and M. Small, "Synchronization of chaotic systems and their machine-learning models," Phys. Rev. E **99**, 042203 (2019).
[5] J. Lü, T. Zhou, and S. Zhang, "Chaos synchronization between linearly coupled chaotic systems," Chaos, Solitons Fractals **14**, 529–541 (2002).
[6] M. Schröder, M. Mannattil, D. Dutta, S. Chakraborty, and M. Timme, "Transient uncoupling induces synchronization," Phys. Rev. Lett. **115**, 054101 (2015).
[7] I. Leyva, I. Sendiña-Nadal, R. Sevilla-Escoboza, V. Vera-Avila, P. Chholak, and S. Boccaletti, "Relay synchronization in multiplex networks," Sci. Rep. **8**, 8629 (2018).
[8] L. M. Pecora and T. L. Carroll, "Master stability functions for synchronized coupled systems," Phys. Rev. Lett. **80**, 2109 (1998).
[9] T. Njougouo, V. Camargo, P. Louodop, F. Fagundes Ferreira, P. K. Talla, and H. A. Cerdeira, "Dynamics of multilayer networks with amplification," Chaos **30**, 123136 (2020).
[10] M. A. Kose, E. S. Prasad, and M. E. Terrones, "How does globalization affect the synchronization of business cycles?," Am. Econ. Rev. **93**, 57–62 (2003).
[11] J. A. Acebrón, L. L. Bonilla, C. J. P. Vicente, F. Ritort, and R. Spigler, "The Kuramoto model: A simple paradigm for synchronization phenomena," Rev. Mod. Phys. **77**, 137 (2005).
[12] N. Chopra and M. W. Spong, "On synchronization of Kuramoto oscillators," in *Proceedings of the 44th IEEE Conference on Decision and Control* (IEEE, 2005), pp. 3916–3922.
[13] N. Fujiwara, J. Kurths, and A. Díaz-Guilera, "Synchronization in networks of mobile oscillators," Phys. Rev. E **83**, 025101 (2011).
[14] R. Guo and Y. Qi, "Partial anti-synchronization in a class of chaotic and hyperchaotic systems," IEEE Access **9**, 46303–46312 (2021).
[15] S. Banerjee, *Chaos Synchronization and Cryptography for Secure Communications: Applications for Encryption* (IGI Global, 2010).
[16] W. Ren, R. W. Beard, and E. M. Atkins, "A survey of consensus problems in multi-agent coordination," in *Proceedings of the 2005 American Control Conference* (IEEE, 2005), pp. 1859–1864.
[17] R. Olfati-Saber, J. A. Fax, and R. M. Murray, "Consensus and cooperation in networked multi-agent systems," Proc. IEEE **95**, 215–233 (2007).
[18] H. Zhang, F. L. Lewis, and A. Das, "Optimal design for synchronization of cooperative systems: State feedback, observer and output feedback," IEEE Trans. Autom. Control **56**, 1948–1952 (2011).
[19] M. M. Al-Sawalha and M. S. M. Noorani, "Anti-synchronization of two hyperchaotic systems via nonlinear control," Commun. Nonlinear Sci. Numer. Simul. **14**, 3402–3411 (2009).
[20] M. El-Dessoky, "Synchronization and anti-synchronization of a hyperchaotic Chen system," Chaos, Solitons Fractals **39**, 1790–1797 (2009).
[21] B. Naderi and H. Kheiri, "Exponential synchronization of chaotic system and application in secure communication," Optik **127**, 2407–2412 (2016).
[22] B. Naderi, H. Kheiri, A. Heydari, and R. Mahini, "Optimal synchronization of complex chaotic T-systems and its application in secure communication," J. Control Autom. Electr. Syst. **27**, 379–390 (2016).
[23] G. Rigatos and M. Abbaszadeh, "Nonlinear optimal control and synchronization for chaotic electronic circuits," J. Comput. Electron. **20**, 1050–1063 (2021).
[24] G. Rigatos and M. Abbaszadeh, "Synchronization of chaotic electronic circuits using nonlinear optimal control," in *2019 IEEE 28th International Symposium on Industrial Electronics (ISIE)* (IEEE, 2019), pp. 670–675.
[25] M. Shi, H. Yuan, and Y. Yuan, "Guaranteed cost optimal leader-synchronization strategy design for distributed multi-agent systems with input saturation," Int. J. Robust Nonlinear Control **32**, 3771–3787 (2022).
[26] G. Rigatos, K. Busawon, and M. Abbaszadeh, "A nonlinear optimal control approach for the truck and N-trailer robotic system," IFAC J. Syst. Control **20**, 100191 (2022).
[27] M. Rafikov and J. M. Balthazar, "On control and synchronization in chaotic and hyperchaotic systems via linear feedback control," Commun. Nonlinear Sci. Numer. Simul. **13**, 1246–1255 (2008).
[28] Z. Liu, "Design of nonlinear optimal control for chaotic synchronization of coupled stochastic neural networks via Hamilton–Jacobi–Bellman equation," Neural Netw. **99**, 166–177 (2018).
[29] O. E. Rössler, "Continuous chaos—Four prototype equations," Ann. N. Y. Acad. Sci. **316**, 376–392 (1979).
[30] F. C. Moon, "*Chaotic Vibrations: An Introduction for Applied Scientists and Engineers* (Wiley, 1987), Vol. 1, pp. 1–309.
[31] A. El-Gohary and A. Sarhan, "Optimal control and synchronization of Lorenz system with complete unknown parameters," Chaos, Solitons Fractals **30**, 1122–1132 (2006).
[32] H. K. Khalil and J. W. Grizzle, *Nonlinear Systems* (Prentice Hall, Upper Saddle River, NJ, 2002), Vol. 3.
[33] L. Tang, X. Wu, J. Lü, J.-A. Lu, and R. M. D'Souza, "Master stability functions for complete, intralayer, and interlayer synchronization in multiplex networks of coupled Rössler oscillators," Phys. Rev. E **99**, 012304 (2019).
[34] M. G. Rosenblum, A. S. Pikovsky, and J. Kurths, "Phase synchronization of chaotic oscillators," Phys. Rev. Lett. **76**, 1804 (1996).
[35] A. S. Pikovsky, M. G. Rosenblum, G. V. Osipov, and J. Kurths, "Phase synchronization of chaotic oscillators by external driving," Physica D **104**, 219–238 (1997).
[36] T. Njougouo, G. R. Simo, P. Louodop, H. Fotsin, and P. K. Talla, "Effects of intermittent coupling on synchronization," Chaos, Solitons Fractals **139**, 110082 (2020).
[37] R. Femat, C. Jiménez, S. Bowong, and G. Solís-Perales, "Accounting the control effort to improve chaos suppression via robust adaptive feedback," Int. J. Model. Identif. Control **6**, 147–155 (2009).
[38] P. Louodop, H. Fotsin, S. Bowong, and A. S. T. Kammogne, "Adaptive time-delay synchronization of chaotic systems with uncertainties using a nonlinear feedback coupling," J. Vibr. Control **20**, 815–826 (2014).
[39] C. Edwards, S. K. Spurgeon, and R. J. Patton, "Sliding mode observers for fault detection and isolation," Automatica **36**, 541–553 (2000).